Quantitative and localized spectroscopy for non-invasive bilirubinometry in neonates

Bosschaart, N.

Publication date
2012

CHAPTER 6

In vivo low-coherence spectroscopic measurements of local hemoglobin absorption spectra in human skin

Localized spectroscopic measurements of optical properties are invaluable for diagnostic applications that involve layered tissue structures, but conventional spectroscopic techniques lack exact control over the size and depth of the probed tissue volume. We show that low-coherence spectroscopy (LCS) overcomes these limitations by measuring local attenuation, and absorption coefficient spectra in layered phantoms. In addition, we demonstrate the first *in vivo* LCS measurements of the human epidermis and dermis only. From the measured absorption in two distinct regions of the dermal microcirculation, we determine total hemoglobin concentration (3.0±0.5 g/L and 7.8±1.2 g/L) and oxygen saturation.

This work has been published in: N. Bosschaart, D.J. Faber, T.G. van Leeuwen and M.C.G. Aalders, "*In vivo* low-coherence spectroscopic measurements of local hemoglobin absorption spectra in human skin", *Journal of Biomedical Optics* 16(10), 100504 (2011)

6.1 Introduction

The derivation of physiological parameters from the spectroscopic determination of tissue optical properties can offer a fast and painless alternative to invasive diagnostic procedures such as tissue biopsies and drawing of blood. For instance, the absorption coefficient of the dermal microcirculation is directly related to the tissue hemoglobin concentration, which provides information on oxygen saturation, blood volume and potentially the hemoglobin concentration in whole blood. A variety of spectroscopic techniques is available for measuring tissue optical properties [1,2]. However, these techniques have limited ability to confine their probing volume to embedded structures such as the dermal microcirculation (which is located beneath the epidermis), or require long photon path lengths (several mm to cm) which exceed the adult dermal thickness of approximately 0.2–1.2 mm [3]. Consequently, many of those techniques rely on assumption-based algorithms to account for layered media [4]. Low-coherence interferometry techniques, such as low-coherence spectroscopy (LCS) [5,6] and spectroscopic optical coherence tomography (sOCT) [7,8] do not suffer from this limitation, since they control the size and position of the probed volume from which the optical properties are determined (lateral and in depth) – i.e. they reject the detection of photons that originate from outside the volume of interest.

In Chapters 4 and 5 we validated LCS on homogeneous phantoms with controlled optical properties, to quantitatively obtain the attenuation $\boldsymbol{\mu_t}$, absorption $\boldsymbol{\mu_a}$ [5], scattering $\boldsymbol{\mu_s}$ and backscattering $\boldsymbol{\mu_b}$ [6] coefficients between 480–700 nm (bold-faced characters denote wavelength (λ) dependent parameters). In this Chapter we present, for the first time to our knowledge, quantitative measurements of local $\boldsymbol{\mu_t}$ and $\boldsymbol{\mu_a}$ spectra within selected volumes of inhomogeneous turbid media. The selection of a volume of interest is supported by a high resolution OCT image that is reconstructed from the LCS signal. We validate our method by retrieving the dye concentration from the measured $\boldsymbol{\mu_a}$ of an Intralipid-dye phantom ($\boldsymbol{\mu_s}$ = 4–6 mm^{-1}, $\boldsymbol{\mu_a}$ = 0–5 mm^{-1}), covered by light attenuating layers with varying optical densities (0.39–0.89). Subsequently, we demonstrate the first *in vivo* LCS measurements of $\boldsymbol{\mu_t}$ and $\boldsymbol{\mu_a}$ of the human epidermis and dermal microcirculation, from which we determine total hemoglobin concentrations and oxygen saturation.

6.2 Materials and methods

6.2.1 System and acquisition

To obtain the $\boldsymbol{\mu_t}$ and $\boldsymbol{\mu_a}$ from a target volume, we measured back scattered power spectra $\mathbf{S}(\ell)$ at controlled geometrical path lengths ℓ of the light in the medium (path length and depth related parameters in this Chapter are corrected for the group refractive index n_g of the medium). Our LCS system, which is described in detail in Chapter 4 [5], consists of a Michelson interferometer and is optimized for the wavelength range of 480–700 nm. We controlled ℓ by translating the reference mirror in steps of 27 μm. By translating the sample in the axial direction, focus tracking of the spot size (r = 4.5 μm) in the medium is achieved. Around ℓ, the signal is modulated by

scanning the piezo-driven reference mirror (23 Hz), resulting in a scanning window of $\Delta\ell \approx 44$ µm in the medium. The optical power at the sample is 6 mW.

A multimode fiber (ø=62.5 µm) guides the reflected light from both arms to a photodiode. Fourier transformation of the acquired time signal results in spectra **S**(ℓ) with spectral resolution $\Delta\lambda = \lambda^2/(n\Delta\ell)$ (4nm < Δλ < 9nm) [5]. To minimize the influence of speckle noise on **S**(ℓ), we spatially average **S**(ℓ) (90-250 spectra) by translating the sample and measuring **S**(ℓ) at every 5 µm. Fitting the single exponential decay model $\mathbf{S}(\ell) = \boldsymbol{\alpha}\cdot\exp(-\boldsymbol{\mu_t}\cdot\ell)$ (free running fit parameters **α** and $\boldsymbol{\mu_t}$) to the background corrected **S**(ℓ) vs. ℓ, results in a $\boldsymbol{\mu_t}$ spectrum [6]. Uncertainties in **α** and $\boldsymbol{\mu_t}$ are estimated by their 95% confidence intervals (c.i.).

6.2.2 Separation of μ_s and μ_a

When **S**(ℓ) is dominated by single backscattered light, the attenuation coefficient $\boldsymbol{\mu_t} = \boldsymbol{\mu_s} + \boldsymbol{\mu_a}$. Since the dependence of $\boldsymbol{\mu_s}$ on wavelength can be described by $a\cdot\lambda^{-b}$, least-squares fitting of $\boldsymbol{\mu_t} = a\cdot\lambda^{-b} + \sum_i (c_i\cdot\boldsymbol{\mu_{a,i}})$ to the wavelength dependent $\boldsymbol{\mu_t}$–measurement results in the individual contributions of $\boldsymbol{\mu_s}$ and $\boldsymbol{\mu_a}$ to the measured $\boldsymbol{\mu_t}$. The free running fit parameters a, b and c_i are constraint to positive values. The wavelength dependent $\boldsymbol{\mu_{a,i}}$ are the known absorption spectra (unit: mm^{-1} per unit concentration) of the contributing chromophores i with contribution c_i, which are the $\boldsymbol{\mu_a}$ of the dye for the phantom measurements and the $\boldsymbol{\mu_a}$ of deoxygenized hemoglobin (Hb) and oxygenized hemoglobin (HbO_2) for the *in vivo* skin measurements [9]. The $\boldsymbol{\mu_a}$ of the dye was obtained from a transmission measurement as described in Chapter 4 [5]. Since we are primarily interested in the total hemoglobin concentration ($[tHb]=c_{HbO2}+c_{Hb}$) and the oxygen saturation ($SO_2=c_{HbO2}/[tHb]$) with their uncertainty estimates (±95%c.i.) for the *in vivo* measurements, we directly fit the [tHb] and the SO_2 by substituting $c_{HbO2}=SO_2\cdot[tHb]$ and $c_{Hb}=(1-SO_2)\cdot[tHb]$ in the fitting algorithm.

6.2.3 OCT image reconstruction

The volume from which we obtain $\boldsymbol{\mu_t}$ is controllable in both size and position inside the medium, by choosing the region for lateral averaging and the ℓ-interval for fitting the exponential decay model. When measuring on inhomogeneous media such as skin, spatial information is needed to confine our region of interest to e.g. the epidermal or dermal layer. Therefore, we support our analysis by reconstructing an OCT image from the individual LCS time signals ($i_{AC}(t)$) within every Δℓ in the axial and lateral direction, using depth scaling d=ℓ/2. The axial resolution of these 'fused' OCT images is given by the coherence length of the light source of ~1.5µm and is therefore higher than the axial resolution of 22µm for **S**(ℓ).

6.2.4 Layered phantoms and in vivo *skin measurement*

We measured $\boldsymbol{\mu_t}$ on a medium consisting of 1% Intralipid (Intralipid®20%, Fresenius Kabi, Germany) and 10% magenta dye (Ecoline #337, Royal Talens, The Netherlands), uncovered and covered by non-absorbing silicone-titanium dioxide (TiO_2) layers [10]. The three covering layers varied in thickness D and scattering, resulting in optical densities ($\mathbf{OD}=D\cdot\boldsymbol{\mu_t}$) of 0.39–0.89 (Table 6.1). The measurement volume (1250x484µm², width x depth) from which we acquired $\boldsymbol{\mu_t}$ was confined to the Intralipid-dye medium, directly behind the layer-medium interface.

For the *in vivo* measurement, we measured the skin of a healthy human volunteer on the palmar side of a stretched finger joint. **S**(ℓ) was acquired over a skin volume of 2000x800 μm^2 (width x depth). During the measurement, the finger joint was stabilized with light pressure against a glass slide. Index-matching gel (Euroband Pedicat, Pollak, France) was applied at the glass-tissue interface to minimize specular reflections.

Table 6.1 *Phantom layer properties and fitted coefficients on the Intralipid-dye medium behind each layer*

	D (μm)	μ_t (mm^{-1})	**OD** ([])	fitted b ([])	fitted dye concentration (%)
no layer	-	-	-	1.8±0.1	10.2±0.5%
layer 1	155	2.5	0.39	1.8±0.2	9.3±0.7%
layer 2	170	5	0.85	1.6±0.2	9.2±0.9%
layer 3	355	2.5	0.89	1.1±0.3	9.3±0.6%

6.3 Results and discussion

6.3.1 Layered phantoms

Figure 6.1 shows the measured μ_t (dots) on the Intralipid-dye medium, uncovered and covered by the three layers with varying **OD**. The μ_t agree within ~10% of the measured values, indicating that the measurement of μ_t is unaffected by the optical density of the layer covering the medium. Also the fits on μ_t (solid lines) and the μ_s-contribution to the fits (dotted lines) are minimally affected by the covering layers. We chose not to separately show the μ_a-contribution to the fits, since this contribution is visible in Figure 6.1 as the difference between the fits on μ_t and their μ_s-contribution. Fitted scatter powers b on the μ_t of the Intralipid-dye medium ranged from 1.1±0.3 to 1.8±0.2 (Table 6.1). The fitted dye concentration ranged between 9.2±0.9% and 10.2±0.5%, resulting in a maximum deviation of 0.8% from the expected dye concentration of 10%.

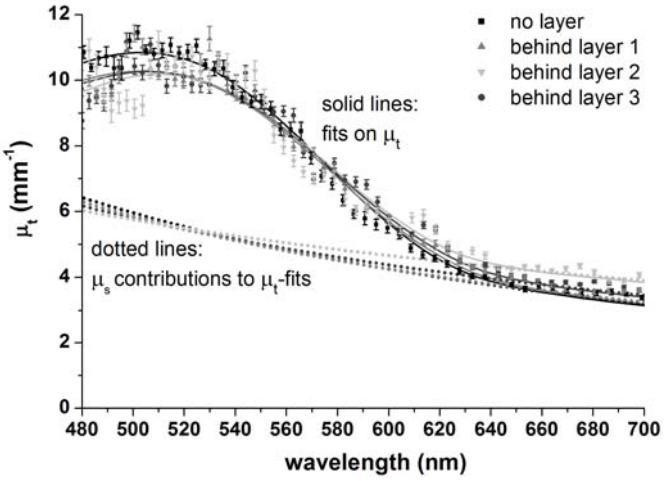

Figure 6.1 *Measured μ_t (dots) of a 1%Intralipid-10%dye phantom behind no layer and three TiO_2-silicone layers with varying **OD** (Table 6.1). Fits on μ_t, and μ_s-contributions to the μ_t-fits are shown for all measurements.*

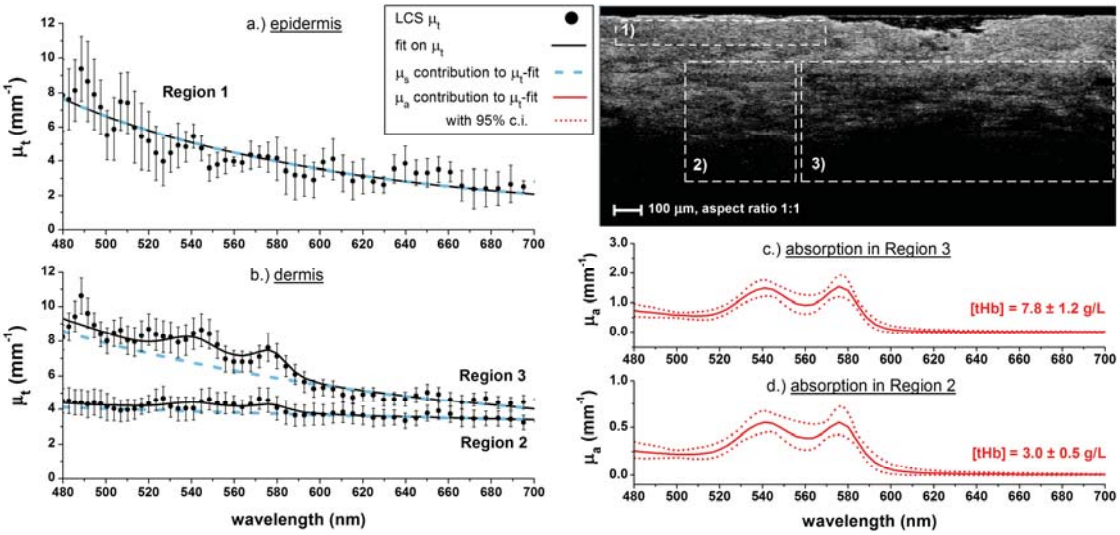

Figure 6.2 *In vivo measurement on the skin of the palmar side of a finger joint. The measured* μ_t*, fits on* μ_t *and* μ_s*-contributions to the* μ_t*-fits are shown in a.) for the epidermis (Region 1) and b.) for the dermis (Regions 2 and 3). The* μ_a*-contributions to the* μ_t*-fits are shown in c.) for Region 3 and d.) Region 2 (note the difference in vertical axis scaling). The selected regions are shown in the OCT image in the upper right corner.*

6.3.2 In vivo *skin measurement*

The upper right corner of Figure 6.2 shows the OCT image that was reconstructed from the *in vivo* measurement on the skin of the palmar side of a stretched finger joint. Using the structural information from the image, we selected regions in the presumed epidermis (Region 1: 715x88μm^2) and dermis (Region 2: 440x418μm^2, Region 3: 1080x418μm^2) for obtaining μ_t. The fit on the measured μ_t of the epidermis (Figure 6.2a) only shows the contribution of scattering (b=3.5±0.3) and neglects the absorption of hemoglobin ([tHb]=0 g/L), which agrees with the expected absence of blood vessels in this skin layer.

Within the dermis, we can distinguish two regions with relatively high (Region 2) and low (Region 3) homogeneity. The measured μ_t differ considerably between the two regions (Figure 6.2b), which can be ascribed to a difference in both scatter power (b=0.5±0.1 in Region 2, b=2.0±0.1 in Region 3) and absorption. The μ_a-spectra of both regions (i.e. the μ_a-contribution to the μ_t-fits) are shown Figure 6.2c and 6.2d. The fitted [tHb] of 3.0±0.5 g/L in Region 2 and 7.8±1.2 g/L in Region 3 indicate the presence of blood and can be related to normal dermal blood volume fractions of 2% and 5% respectively, when assuming a fixed hemoglobin concentration of 150 g/L for whole blood [9]. The fitted SO_2 of 81±34% in Region 2 and 100±31% in Region 3 are also within physiological range.

Presumably, Region 3 encloses a flexure line and Region 2 encloses surrounding skin, since relative differences in hemoglobin absorption up to 63% were found between those two palmar skin regions during stretching [3], which is consistent with our [tHb] results. This also explains the difference in scattering between the two regions, because tissue homogeneity and organization of collagen fiber content, the

major contributor to dermal scattering, differ significantly between these skin regions [3]. The value of the μ_s-contributions to the measured μ_t fall within the physiological range of 1-100 mm^{-1} [1], but the actual dermal μ_s may be underestimated due to the contribution of multiple scattering to the LCS signal [6]. Nevertheless, since absorption takes place along the controlled photon path, this contribution does not influence the determination of μ_a [5].

6.4 Conclusion and outlook

These *in vivo* measurements show that LCS can be used to measure hemoglobin concentration and oxygenation in the microcirculation. Although no gold standard exists to confirm our *in vivo* [tHb] and SO_2 determinations, their values are convincing biologically and the optical properties from which they were derived are within the range of optical properties that were validated in our phantom study. The accuracies at which we determined [tHb] (~15%) and SO_2 (~30%) are influenced by the homogeneity of their distribution within the investigated region, and by the accuracy of the determination of μ_t. The latter is affected by the size of the investigated region (i.e. the number of spatial averages and the length of the ℓ-interval for fitting the exponential decay model) and the **OD** of the medium covering this region, which limits the maximum probing depth of LCS to ~0.5–1 mm *in vivo*. The limiting accuracy of the *in vivo* determination of [tHb] can be expected to be 8%, because this was found to be the minimum accuracy for the determination of the dye concentration in the homogeneous Intralipid-dye layer of the phantoms. Since the epidermal **OD** (~0.8) is comparable to the **OD**'s of the layers in our phantom study, the extra inaccuracy of the [tHb] and SO_2 determination can be ascribed to the skin's heterogeneity [3]. Although the size of the investigated region improves accuracy, it negatively affects measurement speed. Faster acquisition can be achieved by optimizing this trade-off, and by investigating the possibility for Fourier domain acquisition. In contrast to time domain acquisition, the latter will require correction for unwanted signal attenuation due to out-of-focus detection and sensitivity roll-off in depth [8,11].

Potentially, the dermal [tHb] can be related to the hemoglobin concentration in whole blood, if the blood volume within the investigated region can be assessed. A possible method that deserves further investigation for this purpose is obtaining the blood volume from the OCT image by assessing the vessel density using advanced signal analysis, for instance as described in [12]. When measuring on other tissue types, the contribution of additional chromophores (e.g. bilirubin, melanin) to the measured μ_t may need to be incorporated in our algorithm for fitting μ_t. Also correction for Doppler broadening or shifting of the measured μ_t spectra may be needed for tissues that exhibit blood flow. We did not observe any of those influences on the measured μ_t spectra in Figure 6.2b, which can be explained by a temporary decrease of blood flow due to applied pressure on the skin.

In conclusion, we have shown that we can use LCS to locally obtain absorption coefficient spectra within confined volumes of optically inhomogeneous media. This enabled us to perform the first *in vivo* LCS measurements of hemoglobin concentration and oxygen saturation inside the dermal microcirculation. By confining the

measurement volume to specific tissue structures, LCS overcomes the limitations of conventional spectroscopic techniques. LCS therefore offers a potential alternative to invasive drawing of blood for the determination of whole blood hemoglobin concentration and oxygen saturation.

References

1. R. Richards-Kortum, E. Sevick-Muraca, "Quantitative optical spectroscopy for tissue diagnosis", *Annual Review of Physical Chemistry* **47**, 555-606 (1996)
2. R.L.P. van Veen, A. Amelink, M. Menke-Puymers, C. van der Pol, H.J.C.M. Sterenborg, "Optical biopsy of breast tissue using differential path-length spectroscopy", *Physics in Medicine and Biology* **50**, 2573-2581 (2005)
3. T.C. Wright, E. Green, J.B. Phillips, O. Kostyuk, R.A. Brown, "Characterization of a 'blanch-blush' mechano-response in palmar skin", *Journal of Investigative Dermatology* **126**, 220-226 (2006)
4. A. Kienle, M.S. Patterson, N. Dognitz, R. Bays, G. Wagnieres, H. van den Bergh, "Noninvasive determination of the optical properties of two-layered turbid media", *Applied Optics* **37**(4), 779-791 (1998)
5. N. Bosschaart, M.C.G. Aalders, D.J. Faber, J.J.A. Weda, M.J.C. van Gemert, T.G. van Leeuwen, "Quantitative measurements of absorption spectra in scattering media by low-coherence spectroscopy", *Optics Letters* **34**, 3746-3748 (2009)
6. N. Bosschaart, D.J. Faber, T.G. van Leeuwen, M.C.G. Aalders, "Measurements of wavelength dependent scattering and backscattering coefficients by low-coherence spectroscopy", *JBO* **16**, 030503 (2011)
7. D.J. Faber, E.G. Mik, M.C.G. Aalders, T.G. van Leeuwen, "Toward assessment of blood oxygen saturation by spectroscopic optical coherence tomography", *Optics Letters* **30**, 1015-1017 (2005)
8. F.E. Robles, S. Chowdhury, A. Wax, "Assessing hemoglobin concentration using spectroscopic optical coherence tomography for feasibility of tissue diagnostics", *Biomedical Optics Express* **1**, 310-317 (2010)
9. Data tabulated from various sources compiled by S. Prahl, http://omlc.ogi.edu/spectra
10. D.M. de Bruin, R.H. Bremmer, V.M. Kodach, R. de Kinkelder, J. van Marle, T.G. van Leeuwen, D.J. Faber, "Optical phantoms of varying geometry based on thin building blocks with controlled optical properties", *JBO* **15**, 025001 (2010)
11. F. Robles, R.N. Graf, A. Wax, "Dual window method for processing spectroscopic optical coherence tomography signals with simultaneously high spectral and temporal resolution", *Optics Express* **17**, 6799-6812 (2009)
12. L. An, J. Qin and R.K. Wang, "Ultrahigh sensitive optical microangiography for *in vivo* imaging of microcirculations within human skin tissue beds", *Optics Express* **18**, 8220-8228 (2010)